Available online at www.sciencedirect.com
ScienceDirect
Journal of Power Sources 160 (2006) 1287–1293
JOURNAL OF POWER SOURCES
www.elsevier.com/locate/jpowsour

Effect of Co content on performance of $LiAl_{1/3-x}Co_xNi_{1/3}Mn_{1/3}O_2$ compounds for lithium-ion batteries

Shao-Kang Hu [a], Tse-Chuan Chou [a,*], Bing-Joe Hwang [b], Gerbrand Ceder [c]

[a] *Department of Chemical Engineering, National Cheng-Kung University, Tainan, Taiwan, 701*
[b] *Department of Chemical Engineering, National Taiwan University of Science and Technology, Taipei, Taiwan, 106*
[c] *Department of Materials Science and Engineering and Center for Materials Science and Engineering. Massachusetts Institute of Technology, Cambridge, MA 02139-4307, USA*

Received 15 December 2005; received in revised form 2 February 2006; accepted 4 February 2006
Available online 22 March 2006

Abstract

Layered $LiAl_{1/3-x}Co_xNi_{1/3}Mn_{1/3}O_2$ ($0 \leqq x \leqq 1/3$) compounds were studied via the combination of computational and experimental approach. The calculated voltage curve of $LiNi_{1/3}Al_{1/3}Mn_{1/3}O_2$ compound is presented, indicating it is of great potential for a cathode material of lithium-ion batteries. Unfortunately, it was found that the $LiNi_{1/3}Al_{1/3}Mn_{1/3}O_2$ compound without impurity phase could not be synthesized via a sol–gel process. To obtain a layered compound without impurity phase, partial of Al is replaced by Co in $LiNi_{1/3}Al_{1/3}Mn_{1/3}O_2$ compound in this study. Layered $LiAl_{1/3-x}Co_xNi_{1/3}Mn_{1/3}O_2$ ($0 \leqq x \leqq 1/3$) compounds were synthesized via sol–gel reaction at 900 °C under a oxygen stream. Single phase of the $LiAl_{1/3-x}Co_xNi_{1/3}Mn_{1/3}O_2$ in $1/6 \leqq x \leqq 1/3$ region could be prepared successfully. The discharge capacity and conductivity increased with an increase in the Co-substitution content. The enhancement of the conductivity and phase purity by the introduction of Co content shows profound influence on the performance of the $LiAl_{1/3-x}Co_xNi_{1/3}Mn_{1/3}O_2$ compounds.

Keywords: Sol–gel method; First principle calculations; Co content; $LiAl_{1/3-x}Co_xNi_{1/3}Mn_{1/3}O_2$

1. Introduction

Lithium-ion batteries have been well developed as power sources ranging from portable electronic devices to zero-emission vehicles due to their better cycle life and higher energy density than other rechargeable battery systems. Currently, the most widely used commercial cathode material for lithium-ion batteries is $LiCoO_2$ due to its ease of production and stable electrochemical cycling. The relatively high-cost, concerns about the thermal stability of the charged cathode material in electrolyte, and the lure of larger specific capacity has stimulated the study of possible cathode materials for lithium-ion batteries. Recently, manganese based layered compounds as cathode materials for lithium-ion batteries are of great interest and are potential candidates to replace the commercial $LiCoO_2$. These include $LiNi_{1/2}Mn_{1/2}O_2$ [1,2], $LiNi_{1/3}Co_{1/3}Mn_{1/3}O_2$ [3–7] and its derivatives such as $LiNi_xCo_{1-2x}Mn_xO_2$ ($0 \leqq x \leqq 1/3$) [8–10]. The electrochemical processes involve the redox pair of Ni^{+2}/Ni^{+4} with two-electron transfer in the series of these compounds [1,2,5,9].

The optimum electrode material should combine lower cost as well as greater safety and performance compared to $LiCoO_2$. In our recent papers, we showed that $LiNi_{1/3}Co_{1/3}Mn_{1/3}O_2$ may satisfy all of these three criteria [5,7]. Aydinol et al. [11] have reported that $LiAlO_2$ shows a high-calculated potential of 5.4 V versus Li based on the first principle calculations. While pure $LiAlO_2$ is electrochemically inactive, the solid solution of $LiAlO_2$ with various lithiated transition-metal oxides can potentially increase the intercalation voltage and cathode energy density. This effect has recently been confirmed for the $Li_xAl_yCo_{1-y}O_2$, $Li_xAl_yMn_{1-y}O_2$ and $Li_xAl_yCo_zMn_{1-y-z}O_2$ compounds [12–20]. Meanwhile, $LiAlO_2$ is stable in the α-$NaFeO_2$ structure at temperature below ~600 °C [21], suggesting that it could have a stabilizing effect on layered compounds. Its low cost and low density also make $LiAlO_2$ attractive as a constituent of intercalation electrodes.

* Corresponding author. Tel.: +886 6 2007783; fax: +886 6 2366836.
E-mail addresses: tcchou@mail.ncku.edu.tw (T.-C. Chou), bjh@mail.ntust.edu.tw (B.-J. Hwang).

0378-7753/$ – see front matter © 2006 Elsevier B.V. All rights reserved.
doi:10.1016/j.jpowsour.2006.02.005

Motivated by the first principles calculation, the synthesis and characterization of the $LiNi_{1/3}Al_{1/3}Mn_{1/3}O_2$ compound was carried out and compared to those of the $LiNi_{1/3}Co_{1/3}Mn_{1/3}O_2$ in this work. The effect of Co content on the synthesis and electrochemical properties of the $LiAl_{1/3-x}Co_xNi_{1/3}Mn_{1/3}O_2$ compounds will be also investigated.

2. Computational

All calculations are performed in the generalized gradient approximation (GGA) to density functional theory as implemented in the vienna ab initio simulation package (VASP). The nuclei and core electrons are represented with ultra-soft pseudopotentials, and all structures are fully relaxed with respect to internal and external cell parameters. The wave functions are expanded in plane waves with kinetic energy below 400 eV, and Brillouin zone integration is performed with a $6 \times 6 \times 4$ mesh in the supercells with three formula units. Absolute energies were converged with respect to *k*-point sampling. All calculations were performed with spin polarization. Both ferromagnetically and anti-ferromagnetically (anti-parallel) spin polarized was taken into account in the charge density. Partial states of lithiation were investigated at $x = 2/3$, and 1/3 in a supercell with three formula units. There are three distinct Li sites in the supercell with three formula units. Therefore, the number of possible Li arrangements is 1, 3, 3, and 1 corresponding to $x = 1$, 2/3, 1/3, and 0. All the possible arrangements for the supercell with three formula units have been calculated.

3. Experimental

$LiAl_{1/3-x}Co_xNi_{1/3}Mn_{1/3}O_2$ compounds were synthesized by a sol–gel method using a citric acid as a chelating agent. A stoichiometric amount of lithium acetate ($Li(CH_3COO)\cdot 2H_2O$), nickel acetate ($Ni(CH_3COO)_2\cdot 4H_2O$), cobalt nitrate ($Co(NO_3)_2\cdot 6H_2O$), manganese acetate ($Mn(CH_3COO)_2\cdot 4H_2O$) and alumina nitrate ($Al(NO_3)_2\cdot 9H_2O$) were dissolved in distilled water and well mixed aqueous solution of citric acid. The solution was stirred 60–70 °C for 5–6 h to obtain a clear viscous gel. The gel was dried in vacuum oven at 120 °C for 24 h. The materials were precalcined in two stages: at 500 °C for 2 h, and then ground before calcining at high temperature (900 °C) at heating rate of about 5 °C min^{-1}. The powders were slowly cooled to room temperature in oxygen.

Powder X-ray diffraction (XRD) data were collected on a Rigaku diffractometer with Cu Kα radiation ($\lambda = 1.5406$ Å), operating at 300 KV and 60 mA. Grain morphology and particle size of the $LiAl_{1/3-x}Co_xNi_{1/3}Mn_{1/3}O_2$ compounds were examined by scanning electron microscopy using a JEOL JSM-6700. The $LiAl_{1/3-x}Co_xNi_{1/3}Mn_{1/3}O_2$ electrode were fabricated by mixing 85: 1.5: 3.5: 10 (w/w) ratio of active material, KS-6 graphite, Super P carbon black and polyvinylidene fluoride (PVDF), respectively, using *N*-Methyl-pyrrolidone (NMP) as the solvent. The resulting slurry was cast onto an aluminum current collector, dried under vacuum oven for 2 h. The electrode foils were pressed by a roller press to a uniform thickness and then cut into disks of 10 mm diameter. The disk electrode foils were put into an argon filled glove box for conditioning.

Electrochemical measurements were made using coin-type cells comprising Li metal counter electrode and a 1 M solution of $LiPF_6$ in EC/DEC (1:1, v/v) as electrolyte. The cells were assembled in the argon filled glove box where both moisture and oxygen levels are less than 1 ppm. The cells were charged and discharged using a Maccor battery tester at C-rate of C/20 over a potential range between 3.0 and 4.5 V.

4. Results and discussion

4.1. Computational

4.1.1. Density of states of $Li_yNi_{1/3}Al_{1/3}Mn_{1/3}O_2$

The density of states of $LiNi_{1/3}Al_{1/3}Mn_{1/3}O_2$ is shown in Fig. 1. The density of states is presented here for the configuration with lowest total energy. In the lowest energy arrangement Ni and Mn were anti-ferromagnetic. Since the transition-metal ions occupy the octahedral sites in the sublattice of oxygen, the 3d bands of the transition-metal ions are split into the t_{2g} and e_g bands. In $LiNi_{1/3}Al_{1/3}Mn_{1/3}O_2$, the up-spin Ni-$t_{2g}$, Mn-$t_{2g}$ and Ni-e_g bands and down-spin Ni-t_{2g} band are fully occupied corresponding to $Ni - t_{2g}^6 e_g^2$, and $Mn - t_{2g}^3$. It indicates that the oxidation states of Ni, Al and Mn ions are +2, +3 and +4 in $LiNi_{1/3}Al_{1/3}Mn_{1/3}O_2$ compound, respectively. The highest occupied (lowest unoccupied) states are mainly of Ni-e_g (Mn-t_{2g}) character. The band gap of $LiNi_{1/3}Al_{1/3}Mn_{1/3}O_2$ compound is around 0.89 eV, which is higher than 0.63 eV of $LiNi_{1/3}Co_{1/3}Mn_{1/3}O_2$ compound [5], implying the mobility of electrons or holes in $LiNi_{1/3}Al_{1/3}Mn_{1/3}O_2$ compound would be worse than that in $LiNi_{1/3}Co_{1/3}Mn_{1/3}O_2$ compound.

4.1.2. Calculated voltage curve

The open circuit voltage curve can be calculated with well-established methods though it is rather computationally intensive. A reasonable approximation to the voltage curve can be

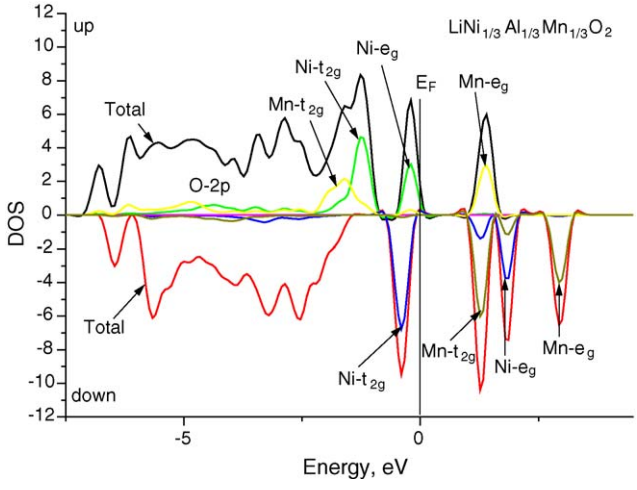

Fig. 1. Density of states of $LiNi_{1/3}Al_{1/3}Mn_{1/3}O_2$.

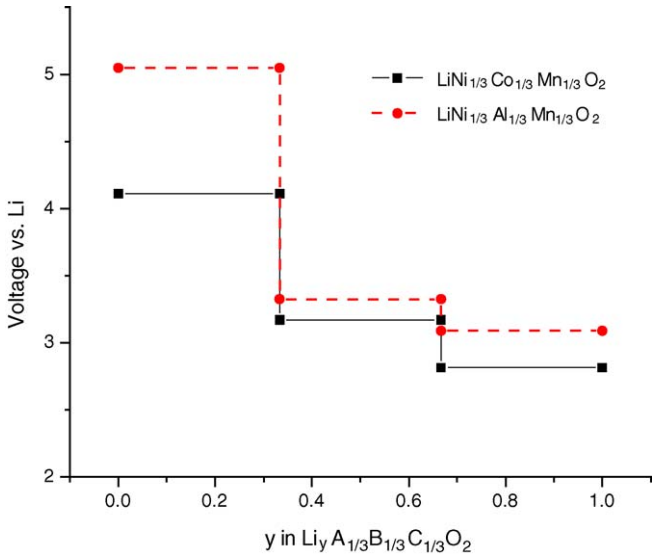

Fig. 2. Calculated average voltage in $Li_xA_{1/3}B_{1/3}C_{1/3}O_2$.

obtained by calculating the average voltage over parts of the Li composition domain. The average voltage for $LiA_{1/3}B_{1/3}C_{1/3}O_2$ in the range of $a \leq y \leq b$ is given as

$$V = \frac{E(Li_aA_{1/3}B_{1/3}C_{1/3}O_2) - E(Li_bA_{1/3}B_{1/3}C_{1/3}O_2) + (b-a)\,E(\mathrm{Lis})}{(b-a)e}$$

The result is given in Fig. 2. One should keep in mind that these voltages are typically under-predicted. The stepwise nature of the voltage curve is not real but arises because the voltage is given as the running average in the domains $n/3 < y < (n+1)/3$ for $n = 0$–2. Given the small voltage variation over the range $1/3 < y < 1$, the true voltage will probably be a gently sloping curve. The redox reaction of Ni^{2+}/Ni^{4+} occurs in this potential range for both $LiNi_{1/3}Al_{1/3}Mn_{1/3}O_2$ and $LiNi_{1/3}Co_{1/3}Mn_{1/3}O_2$ compounds. The calculated voltage for $LiNi_{1/3}Al_{1/3}Mn_{1/3}O_2$ compound is slightly higher than $LiNi_{1/3}Co_{1/3}Mn_{1/3}O_2$ compound in the range of $1/3 < y < 1$, implying $LiNi_{1/3}Al_{1/3}Mn_{1/3}O_2$ compound might provide higher power. For $0 < y < 1/3$, the calculated average voltage for $LiNi_{1/3}Al_{1/3}Mn_{1/3}O_2$ compound is much higher than that for $LiNi_{1/3}Co_{1/3}Mn_{1/3}O_2$ compound. The redox reaction for $LiNi_{1/3}Co_{1/3}Mn_{1/3}O_2$ compound is Co^{3+}/Co^{4+} in this range but the ligand oxygen involves charge transfer for $LiNi_{1/3}Al_{1/3}Mn_{1/3}O_2$ compound [11] in this range. It indicates that it is more difficult to extract all the Li from $LiNi_{1/3}Al_{1/3}Mn_{1/3}O_2$ than $LiNi_{1/3}Co_{1/3}Mn_{1/3}O_2$. The specific capacity for the $LiNi_{1/3}Al_{1/3}Mn_{1/3}O_2$ compound in the range of $1/3 < y < 1$ is calculated to be around 208 mAh g^{-1}, which is higher than 183 mAh g^{-1} for $LiCoO_2$ and the cost of $LiNi_{1/3}Al_{1/3}Mn_{1/3}O_2$ compound is less than the commercial $LiCoO_2$. Considering the benefits of higher capacity, higher power and lower cost, $LiNi_{1/3}Al_{1/3}Mn_{1/3}O_2$ compound is of great potential for the replace of the commercial $LiCoO_2$.

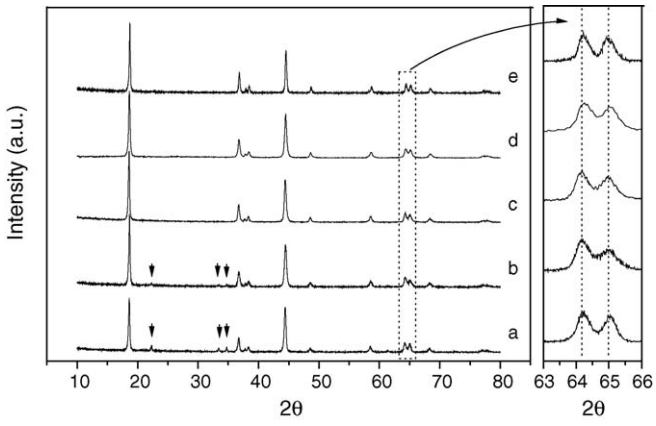

Fig. 3. XRD patterns of $LiAl_{1/3-x}Co_xNi_{1/3}Mn_{1/3}O_2$ powders sintered at 900 °C and the expanded views of the patterns in the section of 63–67°. (a) $x = 0$, (b) $x = 1/12$, (c) $x = 1/6$, (d) $x = 1/4$, (e) $x = 1/3$ (↓: peaks for γ-$LiAlO_2$ phase).

4.2. Experimental

The structure of the $LiNi_{1/3}Al_{1/3}Mn_{1/3}O_2$ powder synthesized by sintering at 900 °C for 2 h was characterized using X-ray diffraction (XRD) (Cu Kα radiation), as shown in Fig. 3a. The peaks for the γ-$LiAlO_2$ phase (tetragonal) are clearly observed in the $LiNi_{1/3}Al_{1/3}Mn_{1/3}O_2$ powder. Since the mixing of the precursors can reach molecular level in the sol–gel process, diffusion and reactions at the sintering temperature would take place without any difficulty. It implies the formation of the $LiNi_{1/3}Al_{1/3}Mn_{1/3}O_2$ powder might be thermodynamically unfavorable. In order to obtain the cathode materials without any impurity phase the Co was introduced to replace Al in the $LiNi_{1/3}Al_{1/3}Mn_{1/3}O_2$ compound. The XRD patterns at various contents of Co in the $LiAl_{1/3-x}Co_xNi_{1/3}Mn_{1/3}O_2$ compounds are shown in Fig. 3b–e. The impurity phase of γ-$LiAlO_2$ is still found in the $LiAl_{1/3-x}Co_xNi_{1/3}Mn_{1/3}O_2$ compound with $x = 1/12$ (Fig. 3b), indicating that its formation is also thermodynamically unfavorable at 900 °C. It was found that single phase of the $LiAl_{1/3-x}Co_xNi_{1/3}Mn_{1/3}O_2$ in $1/6 \leqq x \leqq 1/3$ region could be prepared successfully. The formation of the layered $LiAl_{1/3-x}Co_xNi_{1/3}Mn_{1/3}O_2$ compounds becomes thermodynamically favorable while the substitution of Co is higher than 1/6. The clear splitting of the lines assigned to Miller indices (006, 102) and (108, 110) for the $LiAl_{1/3-x}Co_xNi_{1/3}Mn_{1/3}O_2$ compounds ($1/6 \leqq x \leqq 1/3$) in Fig. 3 indicates good characteristic of layer structure. A partial interchange of occupancy of Li and transition-metal ions would give rise to cation mixing (disordering) in the structure. The R value, the integrated intensity ratio of the (0 0 3)–(1 0 4) lines, is used to measure the degree of cation mixing [9]. The smaller the R value, the higher the disordering. The lower R value means that undesired cation mixing take place. As the Co content x increased, R values are significantly increased from 1.10 to 1.23, as shown in Table 1. These data showed that with an increase in Co content the cation mixing is reduced. In order to illustrate the relation between the unit cell and Co content, x, a- and c-lattice parameters were calculated by the Rietveld refinement method. The best-fitted parameters are given in Table 2 for the $LiAl_{1/3-x}Co_xNi_{1/3}Mn_{1/3}O_2$ compounds.

Table 1
Intensity ratio of I_{003}/I_{104}, cation mixing and electrochemical performance for various samples

Synthesized samples	R value (I_{003}/I_{104})	Theoretical R value (I_{003}/I_{104})	Initial discharge capacity ($mAhg^{-1}$)	Cation mixing
$LiNi_{1/3}Al_{1/3}Mn_{1/3}O_2$	–[a]	1.17	122.5	–
$LiAl_{1/4}Co_{1/12}Ni_{1/3}Mn_{1/3}O_2$	–[a]	1.23	137.2	–
$LiAl_{1/6}Co_{1/6}$ $Ni_{1/3}Mn_{1/3}O_2$	1.10	1.31	153.0	0.069
Li $Al_{1/12}Co_{1/4}$ $Ni_{1/3}Mn_{1/3}O_2$	1.13	1.35	158.0	0.051
$LiNi_{1/3}Co_{1/3}Mn_{1/3}O_2$	1.23	1.40	190.5	0.025

[a] γ-$LiAlO_2$ was observed in XRD measurement.

Obviously, the *a*-axis and *c*-axis increased slightly with increasing the Co content, as shown in Table 2. The lattice variation can be explained by using the crystal lattice parameters of α-$LiAlO_2$ ($a = 2.800$ Å, $c = 14.22$ Å, $R\bar{3}m$) oxide which shows a smaller *a*-axis and c-axis value than those of $LiCoO_2$ [18,22]. Because of the formation of the solid solution between $LiCo_xNi_{1/3}Mn_{1/3}O_2$ and α-$LiAlO_2$ phases, it is reasonable that the *a*-axis and *c*-axis for the $LiAl_{1/3-x}Co_xNi_{1/3}Mn_{1/3}O_2$ compounds increase with an increase in the Co content.

Table 2
Lattice parameters for various samples

Sample	a (Å)	c (Å)	c/a
$LiAl_{1/6}Co_{1/6}Ni_{1/3}Mn_{1/3}O_2$	2.8414	14.1582	4.9828
$LiAl_{1/12}Co_{1/4}Ni_{1/3}Mn_{1/3}O_2$	2.8466	14.1604	4.9745
$LiNi_{1/3}Co_{1/3}Mn_{1/3}O_2$	2.8484	14.1679	4.9740

Fig. 4 shows SEM images of the $LiAl_{1/3-x}Co_xNi_{1/3}Mn_{1/3}O_2$ powders calcined at 900 °C for 2 h after preheating at 500 °C for 2 h: (a) $x = 0$, (b) $x = 1/12$, (c) $x = 1/6$, (d) $x = 1/4$ and (e) $x = 1/3$. The $LiAl_{1/3-x}Co_xNi_{1/3}Mn_{1/3}O_2$ powders ($x = 0$ and 1/12) consist of particles in the form of a smoothly edged polyhedron and round particles with

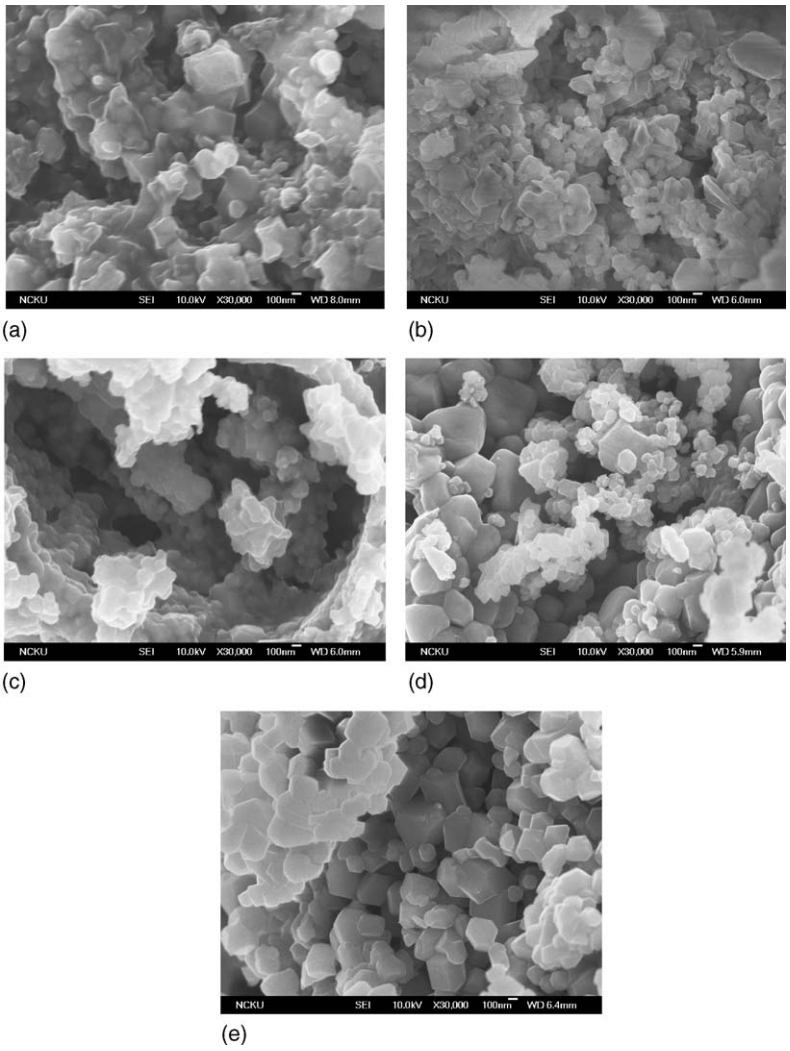

Fig. 4. SEM images of $LiAl_{1/3-x}Co_xNi_{1/3}Mn_{1/3}O_2$ powders sintered at 900 °C. (a) $x = 0$, (b) $x = 1/12$, (c) $x = 1/6$, (d) $x = 1/4$, (e) $x = 1/3$.

relatively small size. The $LiAl_{1/6}Co_{1/6}Ni_{1/3}Mn_{1/3}O_2$ powder comprises secondary agglomeration that is composed of faceted primary particles. The $LiAl_{1/3-x}Co_xNi_{1/3}Mn_{1/3}O_2$ ($x = 1/4$ and 1/3) powders show secondary agglomeration composed of nano-sized and faceted primary particles. The particles of the synthesized $LiAl_{1/3-x}Co_xNi_{1/3}Mn_{1/3}O_2$ compounds ($x = 0$ and 1/12) are obviously composed of a part of γ-$LiAlO_2$ and $Li_{1-z}Al_{1-z}Ni_{1/3}Mn_{1/3}O_2$ crystallite. It is consistent with the observation from XRD. The particle size of the $LiAl_{1/3-x}Co_xNi_{1/3}Mn_{1/3}O_2$ compounds with $x = 0$, 1/12 and 1/6 is smaller than that with $x = 1/4$ and 1/3, indicating the particle size increases with increasing the Co content. The particle size of the $LiAl_{1/3-x}Co_xNi_{1/3}Mn_{1/3}O_2$ compounds with $x = 1/6$, 1/4 and 1/3 is calculated from Scherrer's equation is 35.2, 40.6 and 45.5 nm, respectively. It is also observed the particle morphology from the SEM images that the crystallinity of the synthesized powders becomes better with higher Co content. The particle size distribution of the synthesized $LiAl_{1/3-x}Co_xNi_{1/3}Mn_{1/3}O_2$ powders becomes more uniform at higher Co content. The particle size and crystallinity of the $LiAl_{1/3-x}Co_xNi_{1/3}Mn_{1/3}O_2$ compounds is influenced by the introduction of Co. Since the formation temperature of α-$LiAlO_2$ (∼600 °C) [21] is much lower than $LiNi_{1/3}Co_{1/3}Mn_{1/3}O_2$ (∼900 °C), the formation of γ-$LiAlO_2$ takes place more easily than the layered $Li_{1-z}Co_xNi_{1/3}Mn_{1/3}O_2$ compounds at 900 °C. The formation of γ-$LiAlO_2$ might impede the growth of the $LiAl_{1/3-x}Co_xNi_{1/3}Mn_{1/3}O_2$ particles, which results in the smaller particle size at lower Co content. The substitution of Co can prevent the formation of γ-$LiAlO_2$ and enhance the formation of the layered compounds. Consequently increasing the Co content leads to increase the particle size and crystallinity of the $LiAl_{1/3-x}Co_xNi_{1/3}Mn_{1/3}O_2$ powders. Meanwhile, the better particle size distribution (200∼300 nm) can be obtained at higher Co content.

The $LiAl_{1/3-x}Co_xNi_{1/3}Mn_{1/3}O_2$ ($x = 0$, 1/12, 1/6, 1/4 and 1/3) electrodes cycled in the voltage window of 3.0–4.5 V at a discharge rate of 1/20 C at room temperature is shown in Fig. 5a–e.

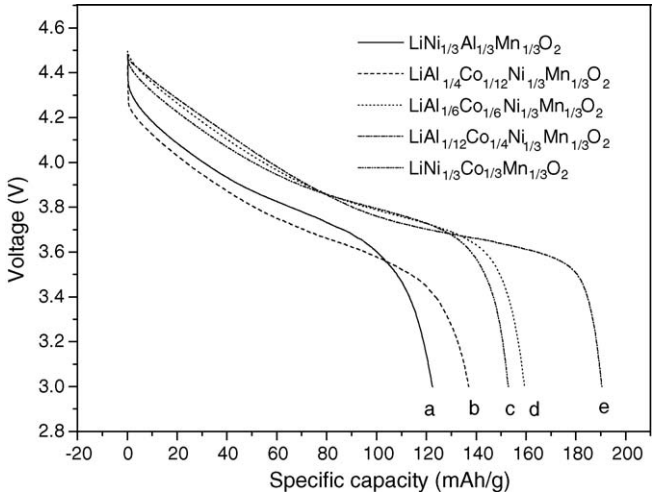

Fig. 5. The first discharge curves of the $LiAl_{1/3-x}Co_xNi_{1/3}Mn_{1/3}O_2$ cells cycled between 3.0 and 4.5 V at 1/20 C rate. (a) $x = 0$, (b) $x = 1/12$, (c) $x = 1/6$, (d) $x = 1/4$, (e) $x = 1/3$.

It was found that the potential drop at the beginning of discharge decreases with an increase in the Co content. Since the potential drop is dominated by the resistance of electronic conduction at the beginning of discharge, indicating that increasing Co content can improve the electronic conductivity of the synthesized compounds. For the $LiAl_{1/3-x}Co_xNi_{1/3}Mn_{1/3}O_2$ ($x = 0$ and 1/12) compounds, the larger potential drop might result from their higher impedance contributed from the formation of the impurity phase of γ-AlO_2. For the $LiAl_{1/3-x}Co_xNi_{1/3}Mn_{1/3}O_2$ ($x = 1/6$, and 1/4) compounds, the large potential drop is associated with their poor electronic conduction, which is in good agreement with the computational results that the band gap of these compounds decreases by the introduction of the Co content.

It is worthy to note that the potential for the $LiAl_{1/3-x}Co_xNi_{1/3}Mn_{1/3}O_2$ compounds ($x = 1/6$ and 1/4) is higher than that of the $LiNi_{1/3}Co_{1/3}Mn_{1/3}O_2$ compound at the middle-discharged state as shown in Fig. 5. It indicates that the substitution of Al can indeed elevate the discharged potential. The results are consistent with the calculated potential curves indicating the discharging potential of the Al-doped compound is higher than that of the $LiNi_{1/3}Co_{1/3}Mn_{1/3}O_2$ compound, as shown in Fig. 2. However, the potential for the $LiAl_{1/3-x}Co_xNi_{1/3}Mn_{1/3}O_2$ compounds ($x = 0$ 1/12, 1/6 and 1/4) is less than that of the $LiNi_{1/3}Co_{1/3}Mn_{1/3}O_2$ compound at the end of discharge, which is in disagreement with the calculated results. The polarization is mainly contributed from the resistance for the diffusion of lithium ions within the particles at the end of discharge. The potential drop decreases with an increase in the Co content at the end of discharge, implying that increasing the Co content can reduce the resistance for the diffusion of lithium ions [23–25]. Since cation mixing would impede the diffusion of lithium ions, it might result from the lower cation mixing of the synthesized compounds at the introduction of higher Co content. The initial discharge capacity of the $LiNi_{1/3}Al_{1/3}Mn_{1/3}O_2$ and $LiAl_{1/4}Co_{1/12}Ni_{1/3}Mn_{1/3}O_2$ compounds is lower than the other samples due to the existence of the impurity phase of γ-$LiAlO_2$. Increasing the Co content of the synthesized compounds leads to reduce their impurity phase, cation mixing and band gap as well as improve their crystallinity. Consequently, the discharge capacity increases with an increase in the Co content, which is mainly contributed from the reduction of the cell polarization. Meanwhile, increasing the Co content in the $LiAl_{1/3-x}Co_xNi_{1/3}Mn_{1/3}O_2$ compounds leads to decrease their irreversible capacity, as shown in Fig. 6. It may result from the improvement of their crystallnity by the introduction of Co.

The electrochemical cycling performance for the $LiAl_{1/3-x}Co_xNi_{1/3}Mn_{1/3}O_2$ electrode materials were tested at the rate of 1/20 C, as shown in Fig. 7 It was obvious that the long-term cyclic performance was improved with an increase in the Co-substitution level. The $LiNi_{1/3}Co_{1/3}Mn_{1/3}O_2$ compound shows the best reversible capacity and cycling performance among the synthesized $LiAl_{1/3-x}Co_xNi_{1/3}Mn_{1/3}O_2$ compounds.

It is suggested from the computational prediction that the $LiNi_{1/3}Al_{1/3}Mn_{1/3}O_2$ compound would show better perfor-

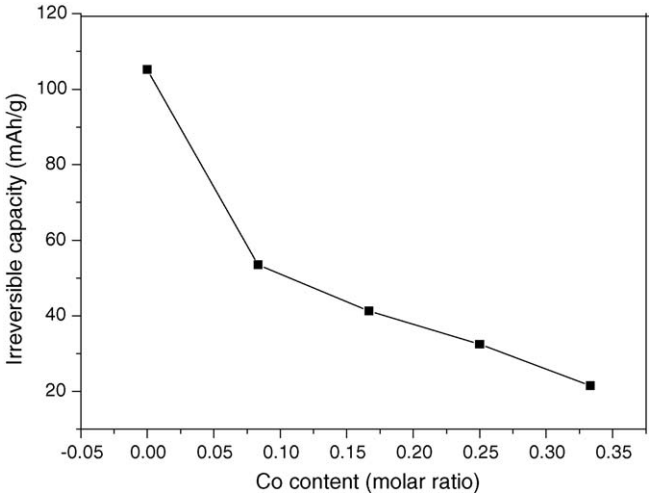

Fig. 6. Effect of Co content on the irreversible capacity of first cycle for the $LiAl_{1/3-x}Co_xNi_{1/3}Mn_{1/3}O_2$ cells cycled between 3.0 and 4.5 V at 1/20 C rate.

mance as a cathode for lithium-ion batteries. However, there is some discrepancy between computational and experimental works. The computation of this study based on a thermodynamic point of view is an ideal approach without considering the effects of cation mixing, electronic conduction, lithium diffusion and charge transfer reaction (kinetics) on the performance of the materials. The substitution of Al for Co in $LiNi_{1/3}Co_{1/3}Mn_{1/3}O_2$ results in increasing the cation mixing, the resistance of electronic conduction, lithium diffusion as well as charge transfer reaction and therefore deteriorating its electrochemical performance. The advantages of high potential and high capacity predicted from the computation for the Al-substituted compounds cannot be achieved due to the kinetic limitation and the suffering from its cation mixing. The better electrochemical performance of $LiNi_{1/3}Al_{1/3}Mn_{1/3}O_2$ compound would be achieved if the processing method can be improved to reduce its cation mixing and impurity phases.

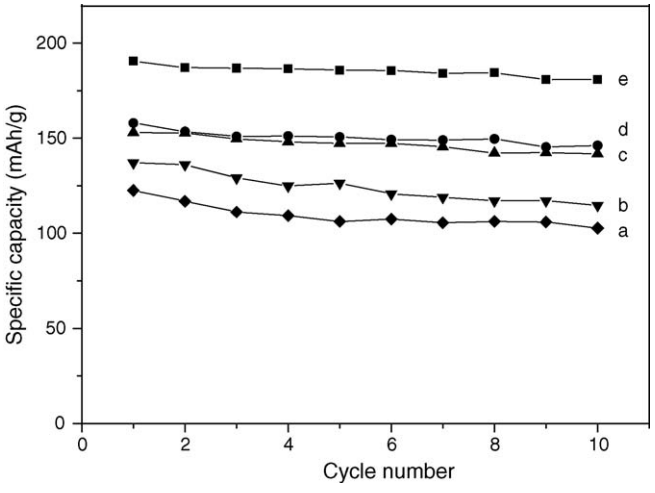

Fig. 7. The specific discharge capacities of the $iAl_{1/3-x}Co_xNi_{1/3}Mn_{1/3}O_2$ cells cycled between 3.0 and 4.5 V at 1/20 C rate. (a) $x = 0$, (b) $x = 1/12$, (c) $x = 1/6$, (d) $x = 1/4$, (e) $x = 1/3$.

5. Conclusions

Layered $LiAl_{1/3-x}Co_xNi_{1/3}Mn_{1/3}O_2$ ($0 \leqq x \leqq 1/3$) compounds were studied via the combination of computational and experimental approach. The $LiNi_{1/3}Al_{1/3}Mn_{1/3}O_2$ compound was predicted from the computational results to show better performance as a cathode for lithium-ion batteries than the $LiNi_{1/3}Co_{1/3}Mn_{1/3}O_2$ compound. The potential for the $LiAl_{1/3-x}Co_xNi_{1/3}Mn_{1/3}O_2$ compounds ($x = 1/6$ and $1/4$) is higher than that of the $LiNi_{1/3}Co_{1/3}Mn_{1/3}O_2$ compound at the middle-discharged state, indicating that the substitution of Al can elevate the discharged potential. The results are consistent with the calculated potential curve. However, there is some discrepancy between computational and experimental works. Increasing the Co content not only reduce the formation of the impurity phase as well as the degree of cation mixing but also improve the crystallinity of the synthesized powders. The electronic polarization and ionic polarization for lithium ion diffusion can be reduced by the introduction of Co in the $LiAl_{1/3-x}Co_xNi_{1/3}Mn_{1/3}O_2$ compounds and therefore results in the better electrochemical properties at the higher Co content. The $LiNi_{1/3}Co_{1/3}Mn_{1/3}O_2$ compound shows the best performance among the synthesized compounds. The advantages of high potential and high capacity predicted from the computation for the Al-substituted compounds can not be achieved due to the kinetic limitation and the suffering from its cation mixing. The performance of the $LiAl_{1/3-x}Co_xNi_{1/3}Mn_{1/3}O_2$ compounds might be improved by optimizing the processing method.

Acknowledgements

Financial support from the Ministry of Education (Ex: 91-EX-FA09-5-4), Taiwan and from National Cheng-Kung University (NCKU) and National Taiwan University of Science and Technology (NTUST), Taiwan, Republic of China are gratefully acknowledged.

References

[1] T. Ohzuku, Y. Makimura, Chem. Lett. 30 (2001) 744.
[2] Y. Koyama, Y. Makimura, I. Tanaka, H. Adachi, T. Ohzuku, J. Electrochem. Soc. 151 (2004) A1499.
[3] T. Ohzuku, Y. Makimura, Chem. Lett. 30 (2001) 642.
[4] K.M. Shaju, G.V. Subba Rao, B.V.R. Chowdari, Electrochim. Acta 48 (2002) 145.
[5] B.J. Hwang, Y.W. Tsai, D. Cariler, G. Ceder, Chem. Mater. 15 (2003) 376.
[6] S.H. Park, C.S. Yoon, S.G. Kang, H.S. Kim, S.I. Moon, Y.K. Sun, Electrochim. Acta 49 (2004) 557.
[7] Y.W. Tsai, B.J. Hwang, G. Ceder, H.S. Sheu, D.G. Liu, J.F. Lee, Chem. Mater. 17 (2005) 3191.
[8] S. Jouanneau, K.W. Eberman, L.J. Krause, J.R. Dahn, J. Electrochem. Soc. 150 (2003) A1637.
[9] S.W. Oh, S.H. Park, C.W. Park, Y.K. Sun, Solid State Ionics 171 (2004) 167.
[10] Y. Sun, C. Ouyang, Z. Wang, X. Huang, L. Chen, J. Electrochem. Soc. 151 (2004) A504.
[11] M.K. Aydinol, A.F. Kohan, G. Ceder, Phys. Rev. B 56 (1997) 1354.
[12] A. Van der Ven, M.K. Aydinol, G. Ceder, G. Kresse, J. Hafner, Phys. Rev. B 58 (1998) 2975.
[13] Q. Zhong, U.V. Sacken, J. Power Sources 54 (1995) 221.

[14] Z. Lu, D.D. MacNeil, J.R. Dahn, Electrochem. Solid-State Lett. 4 (2001) A200.
[15] G. Ceder, Y.M. Chiang, D.R. Sadoway, M.K. Aydinol, Y.-I. Jang, B. Huang, Nature 392 (1998) 694.
[16] T. Ohzuku, A. Ueda, M. Kouguchi, J. Electrochem. Soc. 142 (1995) 4033.
[17] A.M. Kannan, A. Manthiram, J. Electrochem. Soc. 150 (2003) A349.
[18] Y.I. Jang, B. Huang, H. Wang, D.R. Sadoway, G. Ceder, Y.M. Chiang, H. Liu, H. Tamura, J. Electrochem. Soc. 146 (1999) 862.
[19] S.H. Park, K.S. Park, Y.K. Sun, K.S. Sun, K.S. Nahm, Y.S. Lee, M. Yoshio, Electrochim. Acta 46 (2001) 1215.
[20] M. Guilmard, L. Croguennec, C. Delmas, Chem. Mater. 15 (2003) 4484.
[21] V.H.A.Z. Lehmann, H. Hesselbarth, Z. Anorg. Allg. Chem. 313 (1961) 117.
[22] Y.I. Jang, B. Huang, H. Wang, G.R. Maskaly, G. Ceder, D.R. Sodoway, Y.M. Chiang, H. Liu, H. Tamura, J. Power Sources 81 (1999) 589.
[23] T. Ohzuku, A. Ueda, M. Nagayama, Y. Iwakoshi, H. Komori, Electrochim. Acta 38 (1993) 1159.
[24] G.X. Wang, S. Zhong, D.H. Bradhurst, S.X. Dou, H.K. Liu, Solid State Ionics 116 (1999) 271.
[25] Y. Chen, G.X. Wang, K. Konstantinov, H.K. Liu, S.X. Dou, J. Power Sources 119 (2003) 184.